Control and Optimization of a Variable-Pitch Quadrotor with Minimum Power Consumption

Authors:

Shouzhao Sheng, Chenwu Sun

Date Submitted: 2018-11-27

Keywords: variable-pitch quadrotor, adaptive compensation, steady-state identification, steady-state optimization, minimum power consumption

Abstract:

Recently, there has been a rapid growth of interest in quadrotors with electric variable-pitch propellers. The control and optimization of such propellers are important factors for improving the flight performance of the vehicles. Therefore, the steady-state identification method to estimate the parameters of the mathematical model of the electric variable-pitch propeller is developed. The steady-state control and optimization scheme with minimum power consumption and the adaptive compensation scheme for the variable-pitch propeller are then proposed, based on which the response performance of the lift force produced by the variable-pitch propeller can be greatly improved by using a cascade compensation scheme. Furthermore, the direct lift-based flight control strategy is presented, which can significantly contribute to the improvement of the flight performance, precisely because the roll, pitch, yaw and vertical channels of the variable-pitch quadrotor are approximately linearized and completely decoupled from each other in this case. The experimental results demonstrate that both the endurance performance and the positioning accuracy of the variable-pitch quadrotor are improved simultaneously by using the proposed method with minimum power consumption.

Record Type: Published Article

Submitted To: LAPSE (Living Archive for Process Systems Engineering)

Citation (overall record, always the latest version):	LAPSE:2018.0969
Citation (this specific file, latest version):	LAPSE:2018.0969-1
Citation (this specific file, this version):	LAPSE:2018.0969-1v1

DOI of Published Version: https://doi.org/10.3390/en9040232

License: Creative Commons Attribution 4.0 International (CC BY 4.0)

energies

MDPI

Article

Control and Optimization of a Variable-Pitch Quadrotor with Minimum Power Consumption

Shouzhao Sheng * and Chenwu Sun

College of Automation Engineering, Nanjing University of Aeronautics and Astronautics, 29 YuDao St., Nanjing 210016, China; sunchenwu@nuaa.edu.cn

* Correspondence: shengsz@nuaa.edu.cn; Tel.: +86-25-8489-2305

Academic Editor: K.T. Chau

Received: 15 February 2016; Accepted: 18 March 2016; Published: 24 March 2016

Abstract: Recently, there has been a rapid growth of interest in quadrotors with electric variable-pitch propellers. The control and optimization of such propellers are important factors for improving the flight performance of the vehicles. Therefore, the steady-state identification method to estimate the parameters of the mathematical model of the electric variable-pitch propeller is developed. The steady-state control and optimization scheme with minimum power consumption and the adaptive compensation scheme for the variable-pitch propeller are then proposed, based on which the response performance of the lift force produced by the variable-pitch propeller can be greatly improved by using a cascade compensation scheme. Furthermore, the direct lift-based flight control strategy is presented, which can significantly contribute to the improvement of the flight performance, precisely because the roll, pitch, yaw and vertical channels of the variable-pitch quadrotor are approximately linearized and completely decoupled from each other in this case. The experimental results demonstrate that both the endurance performance and the positioning accuracy of the variable-pitch quadrotor are improved simultaneously by using the proposed method with minimum power consumption.

Keywords: minimum power consumption; steady-state optimization; steady-state identification; adaptive compensation; variable-pitch quadrotor

1. Introduction

With the development of small and micro Unmanned Aerial Vehicles (UAVs) in recent years, small, multi-rotor UAVs equipped with electric propellers have gained considerable momentum, and are widely used as experimental and hobby platforms because of their simple mechanical structure, good operability, maneuverability and agility. Therefore, multi-rotor UAVs have recently attracted great interest. Also, considerable work exists on various modeling, design, control, and optimization schemes for multi-rotor UAVs [1–9].

Fixed-pitch multi-rotor designs are mechanically simple. The stability and flight control of fixed-pitch multi-rotors are well established [10–17]. However, the only way to change the lift force produced by a fixed-pitch propeller is by changing the voltage to the motor, which restricts the aggressive and aerobatic maneuvers that multi-rotor UAVs can perform, therefore limiting the applicability of fixed-pitch multi-rotor UAVs in agility-intensive missions [18]. Variable-pitch multi-rotor UAVs can largely overcome the limitations resulting from the fixed-pitch flight.

The benefits of variable-pitch propellers over fixed-pitch propellers for a quadrotor have been analyzed in [19]. The addition of variable-pitch propellers to a quadrotor platform results in an additional degree of freedom for changing the lift produced by each motor-propeller combination. With a variable-pitch propeller, the lift can be changed by either changing the propeller pitch or by changing the rotational speed. These two actuators, to a large extent, overlap, and there are many combinations of rotational

speed and propeller pitch that yield an identical lift. The number of possible combinations is mainly limited by aerodynamic constraints, the maximum propeller pitch and the maximum available motor power. It can be seen from the discussion thus far that on the one hand, the combination could be adjusted to more power efficient settings as the desired lift increases or decreases, and on the other hand, only one combination can yield a desired lift with minimum power consumption. Thus, the control allocation problem of which actuator to use, propeller pitch or rotational speed or combination of the two, needs to be explored systematically under the precondition of ensuring the flight performance, which can certainly contribute to the improvement of the endurance performance of quadrotors.

The modeling and control of the variable-pitch quadrotors have been explored only recently, yet little literature or research is available until now. The design, development, and control of a variable-pitch quadrotor have been studied in [20]. The problem of characterizing the dynamics of a variable-pitch quadrotor from data has been discussed, and black-box versus grey-box models have been analyzed in [21]. The variable-pitch model and the nonlinear proportional squared control algorithm for a quadrotor have also been implemented in the quaternion space [22]. The design of a variable-pitch quadrotor with constant motor speed has been investigated, which has also proven to be most effective in increasing the maneuverability of the quadrotor while largely maintaining its mechanical simplicity [23]. Control and trajectory generation algorithms for a variable-pitch quadrotor have been presented both theoretically and experimentally. The control law is not based on near-hover assumptions, allowing for large attitude deviations from hover [24]. Nevertheless, that research work mainly focused on the aerobatic maneuvers of electric variable-pitch quadrotors. The control and optimization of quadrotors with minimum power consumption has not, to date, been addressed in detail under the precondition of ensuring the flight performance.

The purpose of this study is therefore to develop a proper control and optimization strategy with minimum power consumption for the variable-pitch quadrotor, based on which the endurance performance and the positioning accuracy can be improved. The efficiency and superiority of the proposed method is to be verified by a series of experimental tests.

The structure of the paper is as follows: first, the control and optimization problems are addressed in Section 2, and the steady-state identification method for the variable-pitch propeller is developed in Section 3. Then, the control and optimization strategy for the variable-pitch propeller is presented in Section 4, followed by the direct lift-based flight control strategy for the variable-pitch quadrotor in Section 5. Experimental results are shown in Section 6. Finally, conclusions are drawn in Section 7.

2. The Control and Optimization Problem Statement of the Variable-Pitch Quadrotor

The prototype quadrotor vehicle chosen for this study, 0.5 m in height and 1.45 m in opposite axial distance, is depicted in Figure 1. A maximum take-off mass of 15 kg is assumed including 7 kg of maximum load. The maximum climb speed is approximately 8 m/s while the maximum descent speed is about 13 m/s. The vehicle is used specifically because of the simple mechanical structure, good operability, maneuverability and agility. As the core of the vehicle, the propulsion system mainly consists of an advanced lithium battery, four brushless DC motors, four variable-pitch propellers, and torque-transmitting mechanisms. The variable-pitch propellers driven by the electric motors through the torque-transmitting mechanisms can provide sufficient lift force to lift the vehicle weighing from 8 kg for no load to 15 kg for full load according to the mission equipment.

Figure 1. The variable-pitch quadrotor.

The quadrotor has six degrees of freedom. Let ϕ,θ,ψ represent the roll, pitch and yaw angles of the quadrotor in the inertial frame. Let v_x, v_y, v_z represent the flight velocities of the quadrotor in the body frame. Considering that the flight velocities v_x, v_y are dependent on the attitude θ, ϕ in flight control system design, for simplicity, only the control schemes for ϕ,θ,ψ and v_z are investigated in this study.

The four propellers driven by each motor constitute the propulsion system of the quadrotor. Therefore, the quadrotor has only four control inputs to produce the desired roll, pitch and yaw moments, and the desired vertical movement, as shown in Figure 2, where α_j, ω_j and L_j denote the propeller pitch, the rotational speed and the lift force. Specially, the numerical subscript j indicates different variable-pitch propellers in this paper.

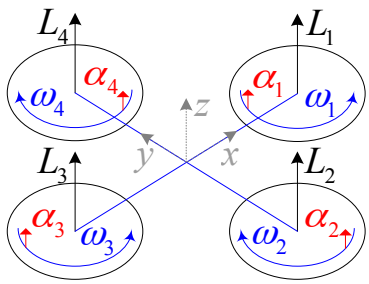

Figure 2. The control inputs and the frames of reference for the variable-pitch quadrotor.

As for the jth control input, the combination of the rotational speed ω_j and the propeller pitch α_j produces the lift force L_j in the direction of the propeller axis as follows [25]:

$$L_j = b_L \alpha_j \omega_j^2 \tag{1}$$

where b_L is an aerodynamic constant, whose estimate, $\hat{b}_L$, can be obtained by using least-squares regression. The total lift force required to produce the movement along the body z axis is then given by:

$$T = \sum_{j=1}^{4} L_j \tag{2}$$

Assuming the variable-pitch quadrotor is near hover, the drag produced by the motor-propeller combination can then be approximately modeled by [25,26]:

$$Q_j = b_{D_1} \alpha_j^2 \omega_j^2 + b_{D_2} \omega_j^2 + b_{D_3} \alpha_j \omega_j \tag{3}$$

where b_{D1}, b_{D2} and b_{D3} can be considered as aerodynamic constants. The torques used to control the roll, pitch and yaw moments can then be described by:

$$T_\phi = l\,(L_4 - L_2) \tag{4a}$$

$$T_\theta = l\,(L_3 - L_1) \tag{4b}$$

$$T_\psi = Q_1 + Q_3 - Q_4 - Q_2 \tag{4c}$$

where l is the horizontal distance from the propeller center to the center of gravity of the quadrotor.

The use of control and optimization of variable-pitch propellers is desirable for a high-performance quadrotor, mainly because on the one hand, the characteristics of the variable-pitch propeller strongly affect the flight dynamics, stability and endurance performance of the vehicle; while on the other hand, any great changes in the gross flight weight with the loads and the flight speed also require the control system to be more complex and more exact. Obviously each motor and propeller has the same characteristics and can be controlled independently. To avoid repetition, the present study is

focused on any pre-specified motor and propeller to demonstrate the proposed control algorithm, which, without loss of generality, can apply to others. For simplicity, the subscript j, denoting the jth motor and propeller, will be omitted in the following two sections, except when there is ambiguity.

3. The Steady-state Identification Method of the Electric Variable-pitch Propeller

The analysis of the basic principle model is crucial for the development of a proper control and optimization scheme to improve the performance of the variable-pitch quadrotor.

The motor is normally modeled by a circuit containing a resistor, inductor, and voltage generator. With regard to the aim of this study, the inductance of a small, brushless hobby motor is negligible when compared to the physical response of the system and so can be ignored. The motor terminal voltage is then approximately given by [27]:

$$u = Ri + \frac{\omega}{K_V} \tag{5}$$

where u is the armature voltage, i is the armature current, R is the armature coil resistance, K_V is the voltage constant, ω is the rotational speed of the motor.

Generally, the motor torque, Q_m, is assumed proportional to the difference between the armature current, i, and the no-load current, i_0, through the torque constant, K_Q:

$$Q_\mathrm{m} = K_Q\left(i - i_0\right) \tag{6}$$

The dynamics of the variable-pitch propeller can then be modeled as a simple first order differential equation:

$$I\dot{\omega} = Q_\mathrm{m} - Q \tag{7}$$

where I is the inertia including the motor and propeller.

Substituting Equations (3), (5) and (6) into Equation (7) yields the following nonlinear differential equation for the electric variable-pitch propeller:

$$I\dot{\omega} + \left(b_{D_1}\alpha^2 + b_{D_2}\right)\omega^2 + \left(b_{D_3}\alpha + b_{D_4}\right)\omega = bu + b_0 \tag{8}$$

where $b_{D_4} = \dfrac{K_Q}{RK_V}, b = \dfrac{K_Q}{R}$ and $b_0 = -K_Q i_0$. Both the armature voltage, u, and the propeller pitch, α, have a substantial effect on the rotational speed of the propeller, thus having a large impact on the lift force of the propeller, which will be discussed in sufficient details in the following section.

However, the control and optimization of the electric variable-pitch propeller is a difficult and often not very precise task, mainly because the coefficients of the differential equation are unknown. As for the steady-state operation, we have:

$$\gamma\left(\alpha, u\right)\Theta = bu \tag{9}$$

where $\gamma\left(\alpha, u\right) = \left[\alpha^2\varpi^2\left(\alpha, u\right), \varpi^2\left(\alpha, u\right), \alpha\varpi\left(\alpha, u\right), \varpi\left(\alpha, u\right), -1\right]$, $\Theta = \left[b_{D_1}, b_{D_2}, b_{D_3}, b_{D_4}, b_0\right]^\mathrm{T}$, and $\varpi\left(\alpha, u\right) = \lim\limits_{t\to\infty} \omega\left(t\right)\Big|_{\substack{\alpha = \text{constant},\\ u = \text{constant}}}$ is the steady-state response to constant inputs.

Considering that the motor rotates in a single direction, which provides sufficient thrust force to lift the quadrotor, the commutation interval angle can be expressed as follows:

$$\vartheta\left(t_k\right) - \vartheta\left(t_{k-1}\right) = 60/N_\mathrm{p} \tag{10}$$

where ϑ denotes the rotational angle; t_{k-1}, t_k denote the $(k-1)$ th and $k$thcommutation instants, respectively, both of which are available from the electric speed controller (ESC) of the motor; N_{p} is the number of pole pairs. The steady-state output, ϖ, can therefore be accurately estimated by:

$$\varpi \approx \frac{60\ell}{N_{\mathrm{p}}\left(t_k - t_{k-\ell}\right)} \tag{11}$$

where ℓ is an optional integral number. On the basis of the discussion made thus far, we can present the steady-state identification algorithm to estimate the coefficients in Equation (8) as follows:

The Steady-state Identification Algorithm:

Input:
The steady-state sample set $S = \{(\alpha_k, u_k, \varpi(\alpha_k, u_k))\}_{k=1}^{n}$, *where the subscript, k , denotes the sample number, and* $n \geqslant 5$. *Moreover, The chosen S satisfies the constraint condition* $\mathrm{cond}\left(\boldsymbol{R}^{\mathrm{T}}\boldsymbol{R}\right) < c_0$, *where* $\boldsymbol{R} = \begin{bmatrix} \gamma(\alpha_1, u_1) \\ \vdots \\ \gamma(\alpha_n, u_n) \end{bmatrix}$, *and* c_0 *is an optional positive value.*

Output:
$\hat{\Theta} = \left[\hat{b}_{D_1}, \hat{b}_{D_2}, \hat{b}_{D_3}, \hat{b}_{D_4}, \hat{b}_0\right]^{\mathrm{T}}$ *and* $\hat{b}$, *which are the estimates of* Θ *and* b, *respectively.*

Steps:

(1) Calculate $\hat{\Theta}_b = \left(\boldsymbol{R}^{\mathrm{T}}\boldsymbol{R}\right)^{-1}\boldsymbol{R}^{\mathrm{T}}\boldsymbol{U}$, *where* $\boldsymbol{U} = \begin{bmatrix} u_1 \\ \vdots \\ u_n \end{bmatrix}$;

(2) Calculate $\hat{b} = \frac{1}{n}\sum_{k=1}^{n}\frac{\gamma(\alpha_k, u_k)\hat{\Theta}_b}{u_k}$;

(3) Calculate $\hat{\Theta} = \hat{\Theta}_b\hat{b}$

As for the DUΛLSKY® XM5060EA-9 (Shanghai Dualsky Models Co., Ltd., Shanghai, China) brushless motor and the 16 inch diameter propeller used in this study, the estimates of the coefficients of the nonlinear differential equation are shown in Table 1 for reference.

Table 1. The estimates of the coefficients of the electric variable-pitch propeller.

Configuration	Variable	Value
XM5060EA-9 motor and 16 inch diameter propeller	$\hat{b}_{D_1}$	2.73×10^{-8}
	$\hat{b}_{D_2}$	1.13×10^{-6}
	$\hat{b}_{D_3}$	2.93×10^{-5}
	$\hat{b}_{D_4}$	2.37×10^{-2}
	$\hat{b}_0$	-2.97×10^{-2}
	$\hat{b}$	0.78

4. The Control and Optimization Strategy for the Electric Variable-Pitch Propeller

4.1. The Steady-State Control and Optimization Scheme with Minimum Power Consumption

As shown in Equation (1), the lift force can be changed by either changing the rotational speed or by changing the propeller pitch. There are many rotational speed and propeller pitch combinations that yield the same lift force values. The optimization of the motor power consumption among the combinations is therefore essential to improve the endurance of the variable-pitch quadrotor. The motor power, P, can be given by:

$$P \approx i^2 R + Q_p \omega \tag{12}$$

The online optimization of the motor power is often an undecidable problem, which, however, can be approximately converted into the minimization of the input voltage to the motor and propeller under the steady-state condition [18]. The solution to the optimization problem can therefore be formulated as follows:

$$(\alpha_c, \omega_c) \approx \underset{L=L_c}{\arg\min}\, u \tag{13}$$

where α_c, ω_c are the sub-optimized propeller pitch command and the sub-optimized rotational speed command of the electric variable-pitch propeller, respectively, and L_c is the lift force command from the flight controller discussed in Section 5.

Not considering the estimation error of the coefficients of the nonlinear differential in Equation (8), the steady-state component of the input voltage can be derived as follows:

$$u_0 = \hat{b}^{-1}\left\{L_c\hat{b}_L^{-1}\left(\hat{b}_{D_1}\alpha_c + \hat{b}_{D_2}\alpha_c^{-1}\right) + L_c^{0.5}\hat{b}_L^{-0.5}\left(\hat{b}_{D_3}\alpha_c^{0.5} + \hat{b}_{D_4}\alpha_c^{-0.5}\right) - \hat{b}_0\right\} \tag{14}$$

According to Equations (1) and (14), the steady-state optimization problem can then be formulated as:

$$\alpha_c \approx \underset{L=L_c}{\arg\min}\left\{L_c^{0.5}\left(\hat{b}_{D_1}\alpha_c + \hat{b}_{D_2}\alpha_c^{-1}\right) + \hat{b}_L^{0.5}\left(\hat{b}_{D_3}\alpha_c^{0.5} + \hat{b}_{D_4}\alpha_c^{-0.5}\right)\right\} \tag{15a}$$

$$\omega_c = \sqrt{\frac{L_c}{\hat{b}_L\alpha_c}} \tag{15b}$$

We therefore conclude that the sub-optimized propeller pitch command, α_c, satisfies the following condition:

$$2\ell_c\left(\hat{b}_{D_1}\beta_c^4 - \hat{b}_{D_2}\right) = \hat{b}_\ell\left(\hat{b}_{D_4}\beta_c - \hat{b}_{D_3}\beta_c^3\right) \tag{16}$$

where $\ell_c = L_c^{0.5}, \hat{b}_\ell = \hat{b}_L^{0.5}$ and $\beta_c = \alpha_c^{0.5}$. It is worth noting that α_c can be obtained online by using the iterative algorithm discussed below. Figure 3 shows the change of the sub-optimized propeller pitch command α_c with the lift force command L_c.

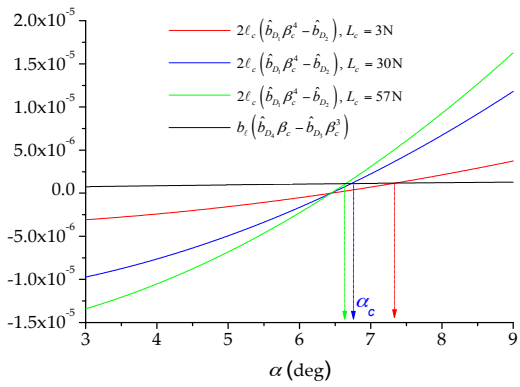

Figure 3. The variation of the sub-optimized propeller pitch command with the lift force command.

The steady-state estimates of the lift force L and the motor power P, as functions of the rotational speed ω and the pitch angle α, can be obtained by using numerical analyses, as shown in Figure 4. The plots show how the lift can be increased by either increasing the rotational speed, increasing pitch, or by increasing both. Given a curve of constant lift force, only one curve of minimum constant motor power remains tangent to it. The black curve indicates the optimal $\alpha - \omega$ trajectory with minimum power consumption, and the sub-optimized propeller pitch command α_c displayed with "X" is comparatively shown in Figure 4. We can conclude that the difference between the sub-optimized propeller pitch and the optimal propeller pitch is insignificant.

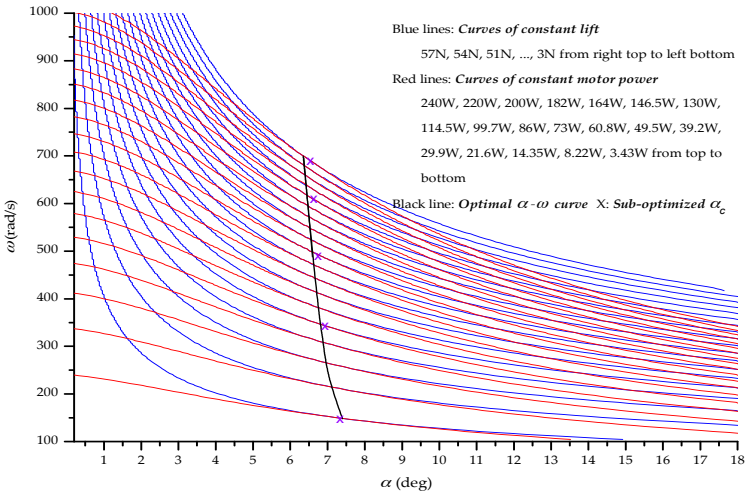

Figure 4. The lift force and the motor power dependences on the rotational speed and the propeller pitch.

Therefore, the motor power consumption is approximately the lowest while changing the propeller pitch and the rotational speed according to Equation (15). Referring to Equation (16) and Figure 3, we then present the online iterative algorithm to optimize the propeller pitch command and the rotational speed command quickly:

The Online Iterative Algorithm:

Input:
$L_c(t_k)$, $\alpha_c(t_{k-1})$ *and* $\Delta\alpha_c$, *where* t_{k-1}, t_k *denote the* $(k-1)$ th *and* kth *control instants, respectively;* $\Delta\alpha_c$ *is the optional minimum increment of* α_c.
Output:
$\alpha_c(t_k)$, $\omega_c(t_k)$.
Steps:(1)
(1) $\alpha_c(t_k) \leftarrow \alpha_c(t_{k-1})$, *and* $i_+, i_- = 0$;
(2) If $i_+ > 0$ *and* $i_- > 0$, *then*
Go to Step 4;
Else
Go to Step 3;
End
(3) If $2\ell_c\left(\hat{b}_{D_1}\beta_c^4 - \hat{b}_{D_2}\right) > \hat{b}_\ell\left(\hat{b}_{D_4}\beta_c - \hat{b}_{D_3}\beta_c^3\right)$, *then*
$\alpha_c(t_k) \leftarrow \alpha_c(t_k) - \Delta\alpha_c$, $i_- \leftarrow i_- + 1$;
Else
$\alpha_c(t_k) \leftarrow \alpha_c(t_k) + \Delta\alpha_c$, $i_+ \leftarrow i_+ + 1$;
End
Return to Step 2;
(4) Calculate $\omega_c(t_k)$.

4.2. The Adaptive Compensation Scheme

We now assume that:

$$u = u_0 + u_a \tag{17}$$

where the adaptive compensation component of the input voltage, u_a, is given by:

$$u_a = \hat{b}^{-1}\left(\hat{b}_{D_1}\alpha_c^2 + \hat{b}_{D_2}\right)\left(\omega^2 - \omega_c^2\right) + \hat{b}^{-1}\left(\hat{b}_{D_3}\alpha_c + \hat{b}_{D_4} - k\right)(\omega - \omega_c) - \hat{b}^{-1}\tilde{k}\omega \tag{18}$$

where k and $\widetilde{k}$ are adjustable parameters. Considering the estimates of the coefficients in Table 1 and the small change of α_c in Figure 3, u_a should be insignificant, as long as $k \approx \hat{b}_{D_4}, \widetilde{k} \approx 0$, and ω is close to ω_c within the normal operating rotational speed range, thus having little effect on the optimization of the electric variable-pitch propeller. Substituting Equations (14), (17) and (18) into Equation (8) yields:

$$\dot{\omega} + \left(k_a + \widetilde{k}_a + \varepsilon_b\right)\omega = k_a \omega_c \tag{19}$$

where $k_a = \hat{I}_b^{-1} k$, $\widetilde{k}_a = \hat{I}_b^{-1}\widetilde{k}$, $\varepsilon_b = \left\{\left(\hat{b}_{D_1}\alpha_c^2 + \hat{b}_{D_2}\right)\omega + \left(\hat{b}_{D_3}\alpha_c + \hat{b}_{D_4}\right) - b\omega^{-1}\right\}\left(I^{-1} - \hat{I}_b^{-1}\right)$, and $\hat{I}_b = I\hat{b}b^{-1}$. Note that ε_b is also insignificant.

Considering that u_a should be insignificant within the normal operating rotational speed range, the ideal model is therefore defined as:

$$\dot{\omega}_m + \hat{k}_m \omega_m = \hat{k}_m \omega_c \tag{20}$$

where $\hat{k}_m = \hat{I}^{-1}\hat{b}_{D_4}$, and $\hat{I}$ is the estimate of I.

The tracking error between the outputs of the plant and the model is then defined as:

$$e = \omega_m - \omega \tag{21}$$

Now, we consider the Lyapunov function candidate:

$$V = e^2 + \lambda_a \delta_a^2 + \widetilde{\lambda}_a \widetilde{\delta}_a^2 \tag{22}$$

where $\delta_a = \hat{k}_m - k_a, \widetilde{\delta}_a = \widetilde{k}_a + \varepsilon_b$, and $\lambda_a, \widetilde{\lambda}_a$ are optional positive values. The derivative of the Lyapunov function candidate is then negative definite as the adaptive laws are presented as follows:

$$\begin{cases} \dot{k} = \gamma_a (e + \mu) e_0 \\ \dot{\widetilde{k}} = -\widetilde{\gamma}_a (e + \mu) \omega \end{cases} \tag{23}$$

where $\gamma_a = \lambda_a^{-1}\hat{I}_b$, $\widetilde{\gamma}_a = \widetilde{\lambda}_a^{-1}\hat{I}_b$, $e_0 = \omega_c - \omega$, and μ satisfies the constraint condition:

$$\mathrm{sgn}(\mu) = \mathrm{sgn}\left(\dot{e} + \hat{k}_m e\right) \tag{24}$$

Note that the term μ can greatly contribute to the convergence rates of adjustable parameters, as can be seen from:

$$\dot{V} = 0.5\left\{-\hat{k}_m e^2 - \left(\dot{e} + \hat{k}_m e\right)\mu\right\} \tag{25}$$

The adaptive compensation given by Equation (23) can reduce the tracking error such that ω is, as far as possible, close to ω_m, thus improving the response performance of the rotational speed.

4.3. The Cascade Compensation Scheme

As described thus far, referring to Equations (1) and (20), we approximately have:

$$\frac{L(s)}{L_c(s)} \approx \frac{a_m}{s + a_m} \tag{26}$$

where $a_m = 2\hat{k}_m$. We can further improve the response performance of the variable-pitch propeller through a single cascade compensation element:

$$\frac{L_c(s)}{L_p(s)} \approx \frac{a_m^{-1}s + 1}{a_p^{-1}s + 1} \tag{27}$$

where a_p is an optional positive value, and L_p is the control signal from the flight controller discussed in Section 5. Therefore:

$$\frac{L(s)}{L_p(s)} \approx \frac{a_p}{s + a_p} \tag{28}$$

It is finally noted that both the adaptive compensation and the cascade compensation can greatly contribute to the improvement of the control quality of the variable-pitch propeller. The control scheme of the variable-pitch propeller, including the steady-state optimization, the adaptive compensation and the cascade compensation, is shown in Figure 5.

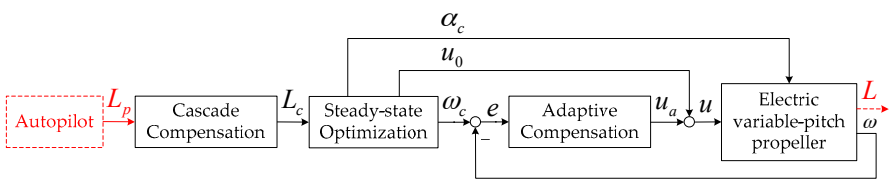

Figure 5. The schematic diagram of the electric variable-pitch propeller.

5. The Direct Lift-based Flight Control Strategy for the Variable-Pitch Quadrotor

5.1. The Direct Lift-based Height Control Scheme

Considering that each motor and propeller has the same input-output properties, according to Equations (2) and (28), the total lift produced by the combined effect of the forces produced by the four propellers can also be expressed by:

$$\frac{T(s)}{T_p(s)} \approx \frac{a_p}{s + a_p} \tag{29}$$

where:

$$T_p = \sum_{j=1}^{4} L_{pj} \tag{30}$$

and L_{pj} denotes the lift command signal corresponding to the jth propeller, as shown in Figure 5.

As for the near-hover flight, we suppose that:

$$T_{ph} = T_p - mg \tag{31a}$$

$$T_h = T - mg \tag{31b}$$

where T_{ph} denotes the control signal from the height controller discussed below, m denotes the mass of the quadrotor, and g denotes the gravitational acceleration. After offsetting the gravity acting on the variable-pitch quadrotor, Equation (29) can then be rewritten by:

$$\frac{T_h(s)}{T_{ph}(s)} \approx \frac{a_p}{s + a_p} \tag{32}$$

Let z, z_c be the actual height and the height command signal, respectively. We propose the direct lift-based height control law as follows:

$$T_{ph} = k_{zp}\varepsilon_z + k_{zi}\int \varepsilon_z \mathrm{d}t - ma_p v_z - T_h \tag{33}$$

where k_{zp}, k_{zi} are optional parameters, and:

$$\varepsilon_z = ma_p\left(z_i - z\right) + m\left(v_{zi} - v_z\right) \tag{34}$$

where z_i is the output of a cascade compensation element in response to z_c; v_{zi} is correspondingly the derivative of z_i.

It is worthy to note that the direct-lift feedback term in Equation (33) can contribute to the stability of the height. The transfer function, from the input z_i to the output z, can then be derived by using the knowledge of rigid-body kinematics and by substituting Equations (33) and (34) into Equation (32) as follows:

$$\frac{z\left(s\right)}{z_i\left(s\right)} \approx \frac{a_p k_{zp} s + a_p k_{zi}}{s^3 + a_p s^2 + a_p k_{zp} s + a_p k_{zi}} \tag{35}$$

The cascade compensation element is further chosen as:

$$\frac{z_i\left(s\right)}{z_c\left(s\right)} \approx \frac{\omega_z^2 s^3 + \omega_z^2 a_p s^2 + \omega_z^2 a_p k_{zp} s + \omega_z^2 a_p k_{zi}}{a_p k_{zp} s^3 + \left(2\xi_z \omega_z a_p k_{zp} + a_p k_{zi}\right) s^2 + \left(\omega_z^2 a_p k_{zp} + 2\xi_z \omega_z a_p k_{zi}\right) s + \omega_z^2 a_p k_{zi}} \tag{36}$$

where ξ_z and ω_z are optional parameters. Thus:

$$\frac{z\left(s\right)}{z_c\left(s\right)} \approx \frac{\omega_z^2}{s^2 + 2\xi_z \omega_z s + \omega_z^2} \tag{37}$$

where ξ_z and ω_z can be considered as the damping and natural frequency. The dynamics of the height is therefore determined by the choices of $k_{zp}, k_{zi}, \xi_z, \omega_z$ and a_p.

5.2. The Direct Lift-based Attitude Control Scheme

As described in Section 2, the moments are produced by generating a differential lift across the two propellers on the same arm of the quadrotor, thus providing the input necessary for the quadrotor to move longitudinally or laterally; for making the quadrotor yaw to a particular orientation, the lifts of a set of opposite propellers are changed simultaneously and by the same amount.

It can be seen from Table 1 that the second term on the right-hand side of Equation (3) remains dominant in the drag produced by the motor-propeller combination. We therefore suppose that:

$$T_{\phi c} = L_{p4} - L_{p2} \tag{38a}$$

$$T_{\theta c} = L_{p3} - L_{p1} \tag{38b}$$

$$T_{\psi c} = L_{p1} + L_{p3} - L_{p4} - L_{p2} \tag{38c}$$

The roll, pitch and yaw channels can then be considered to be approximately linear and decoupled as $T_{\phi c}$, $T_{\theta c}$ and $T_{\psi c}$ are chosen as the control input signals without considering other aerodynamic effects.

We then propose the direct lift-based attitude control laws as follows:

$$T_{\phi c} = k_{\phi p} e_\phi + k_{\phi i} \int e_\phi \mathrm{d}t + k_{\phi d} \dot{e}_\phi - k_{\dot{\phi}} \dot{\phi} \tag{39a}$$

$$T_{\theta c} = k_{\theta p} e_\theta + k_{\theta i} \int e_\theta \mathrm{d}t + k_{\theta d} \dot{e}_\theta - k_{\dot{\theta}} \dot{\theta} \tag{39b}$$

$$T_{\psi c} = k_{\psi p} e_\psi + k_{\psi i} \int e_\psi \mathrm{d}t + k_{\psi d} \dot{e}_\psi - k_{\dot{\psi}} \dot{\psi} \tag{39c}$$

where $e_\phi = \phi_i - \phi$, $e_\theta = \theta_i - \theta$, $e_\psi = \psi_i - \psi$; ϕ_i, θ_i, ψ_i are the roll, pitch and yaw command signals, respectively; $k_{\phi p}, k_{\phi i}, k_{\phi d}, k_{\dot{\phi}}, k_{\theta p}, k_{\theta i}, k_{\theta d}, k_{\dot{\theta}}, k_{\psi p}, k_{\psi i}, k_{\psi d}, k_{\dot{\psi}}$ are optional parameters.

Compared with conventional flight control methods for variable-pitch quadrotors, the direct lift-based flight control method can improve the flight performance, precisely because all channels are approximately linearized and completely decoupled from each other in this case. It is finally noted that the lift command signal to each motor and propeller can be obtained from Equations (30), (31), (33), (38) and (39).

The longitudinal movement is constituted by the forward velocity caused by the pitch angle θ produced by the moment T_θ, and so does the lateral movement. The longitudinal and lateral trajectory controllers are commonly referred to as the outer-loop controllers and can also be easily designed by using conventional linear control techniques, which have been studied in many literatures, such as [4–6], so won't be covered here.

6. Experimental Tests

In this section, we first describe the details of the experimental setup used for verification purposes. Finally, extensive experimental tests are carried out along with necessary discussions and evaluations.

6.1. The Experimental Setup and Description

Apart from the variable-pitch propeller described in Section 2, the component parts of the control system of the quadrotor include a DSP-based hardware platform and a high integrity navigation unit. The software of the proposed control scheme runs at 200 Hz on the DSP-based hardware platform that can provide reliable support for high precision timer and synchronization operations. The flight controller, performing the closed-loop attitude and altitude control module, is employed to generate the command as inputs to the control system of the variable-pitch propeller. The high integrity navigation system, based on the combined use of the Global Positioning System (GPS) and an inertial measurement unit (IMU), is used to provide the flight controller with the accurate attitude, position and velocity information. The discrete estimate of the rotational speed can be obtained by the use of the commutation instant from the ESC since the commutation interval angle is constant, shown in Equation (10), and the rotational speed is high within the normal operating rotational speed range.

To test and verify the efficiency of the proposed control method, the prototype quadrotor is first conducted to repeatedly perform climb and descent flights in attitude hold mode. Figure 6 shows the experimental test scenes for the present study. For simplicity, only the experimental results related to the pre-specified variable-pitch propeller are given to demonstrate the proposed method under the aerodynamic constraints and the power constraints.

(**a**) (**b**)

Figure 6. Experimental test scenes: (**a**) take-off flight; (**b**) climb and descent flights.

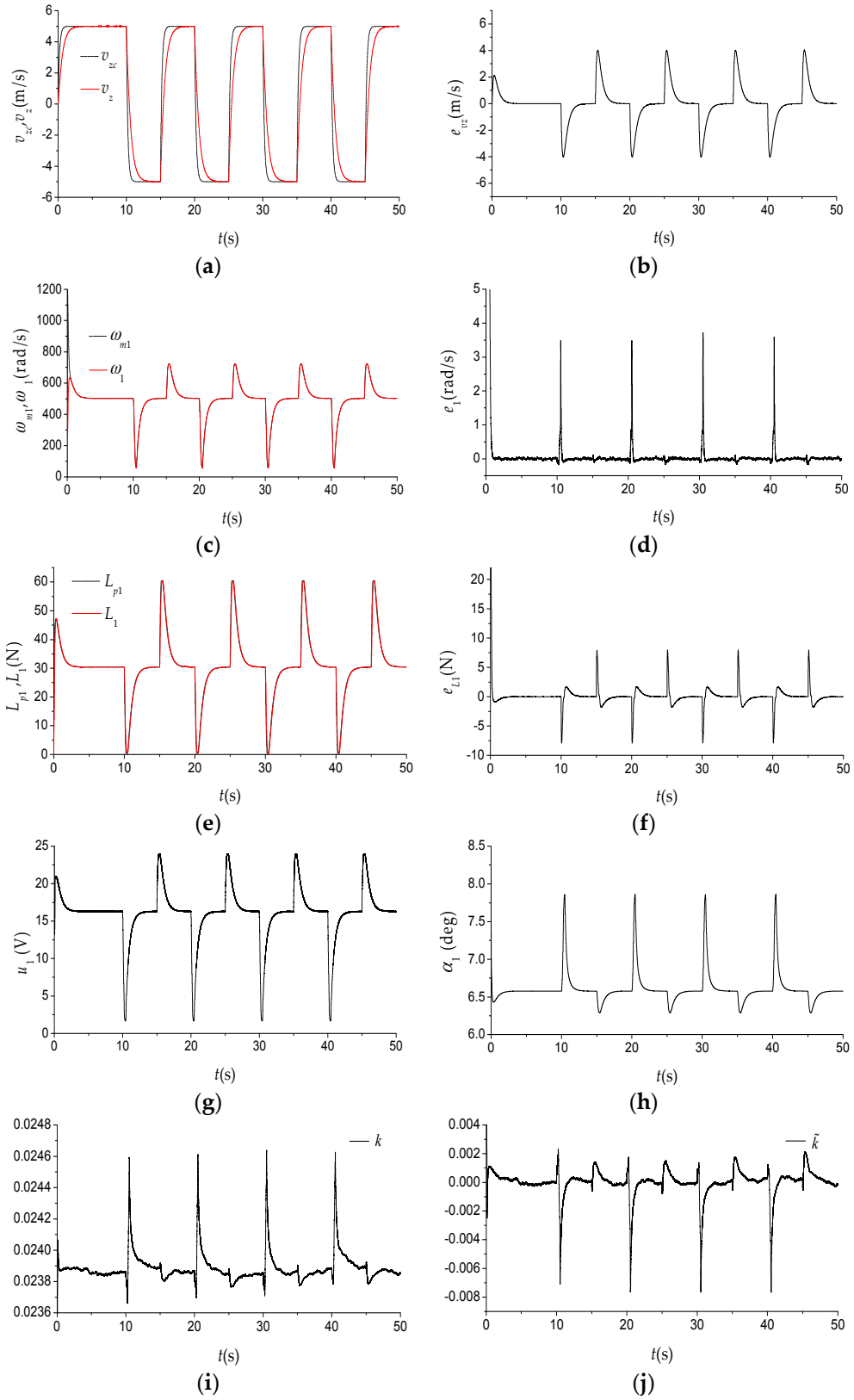

Figure 7. Experimental results of the proposed method in the case of the vertical flight with constant velocity: (**a**) v_{zc} and v_z ; (**b**) e_{vz} ; (**c**) ω_{m1} and ω_1 ; (**d**) e_1 ; (**e**) L_{p1} and L_1 ; (**f**) e_{L1} ; (**g**) u_1 ; (**h**) α_1 ; (**i**) k ; (**j**) $\tilde{k}$. Other propellers have similar characteristics.

6.2. Vertical Flight and Endurance Tests

6.2.1. Experimental Tests of the Proposed Method

The vertical flight tests are conducted to comparatively assess the endurance performance of the variable-pitch quadrotor by using the proposed method and the conventional method. All predefined parameters of the flight control system of the variable-pitch quadrotor are first described as follows:

(1) The estimates of aerodynamic parameters: $\hat{b}_L = 1.75 \times 10^{-5}, \hat{I} = 1.37 \times 10^{-3}$;
(2) Adaptive compensation in the rotational speed loop: $\gamma_a = 1.0 \times 10^{-3}$, $\tilde{\gamma}_a = 1.0 \times 10^{-5}$, $\mu = \dot{e} + \hat{k}_m e$;
(3) Cascade compensation in the lift force loop: $a_p = 5$;
(4) Direct lift-based height control scheme: $k_{zp} = 2.0, k_{zi} = 1.6, \xi_z = 2.0, \omega_z = 0.75$;
(5) Direct lift-based attitude control scheme: $k_{\phi p}, k_{\theta p} = 2.1, k_{\phi i}, k_{\theta i} = 0, k_{\phi d}, k_{\theta d} = 0.5, k_{\dot{\phi}}, k_{\dot{\theta}} = 0.1$, $k_{\psi p} = 9.0, k_{\psi i} = 0.5, k_{\psi d} = 3.0, k_{\dot{\psi}} = 0.5$;
(6) Longitudinal position control scheme: $\theta_i = k_p e_x + k_i \int e_x \mathrm{d}t + k_d \dot{e}_x - k_v v_x$, where e_x is the position error along the body x axis, $k_p = 1.0$, $k_i = 0.1$, $k_d = 0.2$, $k_v = 1.0$, and so does the lateral position control scheme. A series of real-time experimental tests are then conducted based on the above assumptions.

Figure 7 shows the experimental results of the proposed method in the case of the vertical flight with constant velocity, where $z_c(t) = \int_0^t v_{zc}(\tau)\,\mathrm{d}\tau$; v_{zc} is the vertical velocity command signal; e_{vz} is the error between v_{zc} and v_z; e_{L1} is the error between L_{p1} and L_1.

For simplicity, only the results related to the first propeller are shown in the figure. It is seen from Figure 7a–f that the resulting controlled system can achieve good tracking performances, even though the voltage and the propeller pitch exhibit significant variations in accordance with the vertical velocity command signal shown in Figure 7g,h. Meanwhile, the adjustable parameters of the adaptive compensation element also have good convergence properties as shown in Figure 7i,j during the maneuver flights. It is, however, to note that the rotational speed tracking error demonstrates a remarkable difference during the climb flight mode and the descent flight mode due to the nonlinear characteristics of the propeller.

To further demonstrate the positive effect of the propeller pitch on the endurance performance and comparatively assess the efficiency and superiority of the proposed method, the propeller pitch α involved in the proposed method is set equal to α_c and different constant values, respectively, and simultaneously, the variable-pitch quadrotor is particularly equipped with the same type of Lithium battery with a capacity of 5000 mAh for each experimental test. Table 2 and Figure 8 show the endurance performance versus propeller pitch angles using the proposed method.

Table 2. The endurance performance *versus* propeller pitch angles.

Battery Capacity	α(deg)	Endurance (s)
5000 mAh	Sub-optimized value	267.30
	3	155.36
	4	197.50
	5	226.61
	6	246.72
	7	251.65
	8	249.22
	9	246.77
	10	243.27
	11	239.70
	12	234.91
	13	229.19
	14	220.52
	15	212.58

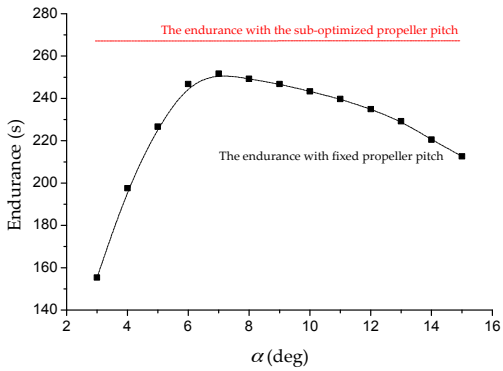

Figure 8. The endurance performance *versus* propeller pitch angles

The proposed method with minimum power consumption has the most significant improving effect on the endurance performance when compared to the fixed propeller pitches. According to the test results, the improvement of the endurance performance of the quadrotor ranges from 6.2% to 72.1%.

6.2.2. Experimental Tests of the Conventional Method with Constant Rotational Speed

In order to make a fair comparison between the proposed method and the conventional method with constant rotational speed implemented through the widely used Pixhawk® autopilot module, the experimental tests of the conventional method are then conducted for this purpose, where the autopilot employs one optimal proportional-integral controller to obtain the armature voltage according to the rotational speed tracking error, and another optimal proportional-integral- differential controller to determine the propeller pitch according to the vertical velocity tracking error.

The predefined parameters are described as follows:

(1) Rotational speed control scheme (optimal proportional-integral control): proportional and integral coefficients equal to 0.85 and 1.95;
(2) Vertical velocity control scheme (optimal proportional-integral-differential control): proportional, integral and differential coefficients equal to 2.5, 1.0 and 0.2.

Figure 9 shows the experimental results with the rotational speed command signal ω_{cj} = 400 (j = 1, 2, 3, 4). The propeller pitch exhibits a significant variation in accordance with the vertical velocity command signal during the maneuver flights, as shown in Figure 9f, although the vertical velocity tracking performance deteriorates slightly and is basically acceptable when compared to the proposed method.

Similarly, to demonstrate the effect of the rotational speed on the endurance performance in this test case, the rotational speed command signal is set equal to different constant values. The experimental tests are conducted with the same equipment as mentioned above, and the resulting endurance performance *versus* rotational speeds is shown in Table 3 and Figure 10.

Table 3. The endurance performance *versus* rotational speeds.

Battery Capacity	ω_c(rad/s)	Endurance (s)
5000 mAh	350	230.95
	400	240.09
	450	239.89
	500	232.52
	550	220.43
	600	205.31
	650	189.06

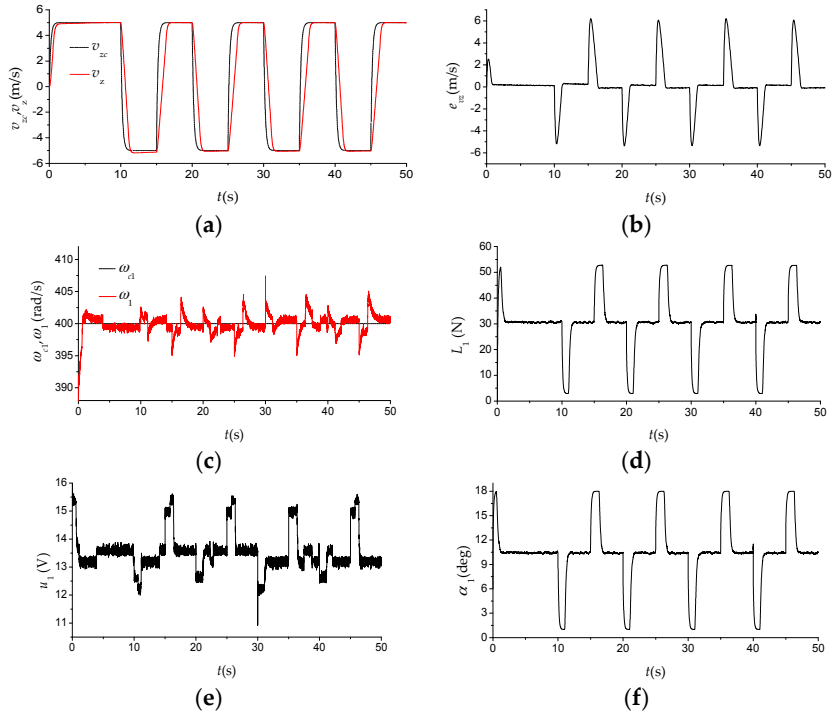

Figure 9. Experimental results of the conventional method with $\omega_{cj} = 400$ ($j = 1, 2, 3, 4$): (**a**) v_{zc} and v_z ; (**b**) e_{vz} ; (**c**) ω_{c1} and ω_1 ; (**d**) L_1 ; (**e**) u_1 ; (**f**) α_1 . Other propellers have similar characteristics.

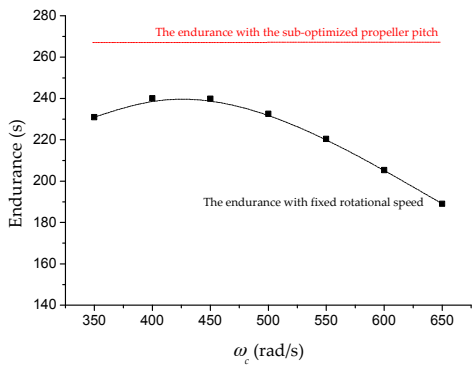

Figure 10. The endurance performance versus rotational speeds.

In contrast to what has been shown in Table 2 and Figure 8, the endurance with fixed rotational speed decreases distinctly, although the control quality is basically satisfactory in practice, which also comparatively demonstrates that the proposed method can contribute to the significant improvement of the endurance performance.

6.3. Positioning Accuracy Tests

All predefined parameters of the proposed algorithm are defined in Section 6.2.1. Figure 11 shows the experimental results of the proposed algorithm during near-hover operations, where v_n, v_e, v_h are the northward, eastward and vertical velocities in the Earth frame. The proposed method can achieve a good trajectory tracking performance when the variable-pitch quadrotor is conducted to perform a low-velocity trajectory tracking task, as shown in Figure 11a–c. Furthermore, according to the experimental data, the deviation distance is less than 0.08 m during the straight line flight, and the height tracking error is less than 0.12 m in the presence of disturbances and uncertainties.

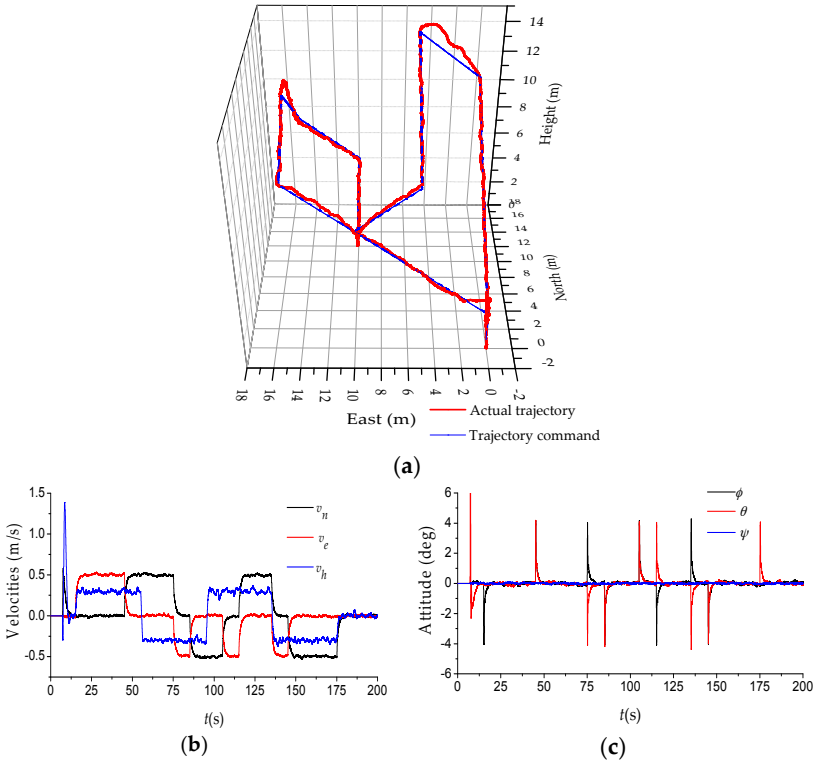

Figure 11. The experimental results of the proposed method during near-hover operations: (**a**) 3D flight trajectory tracking; (**b**) flight velocities; and (**c**) attitude.

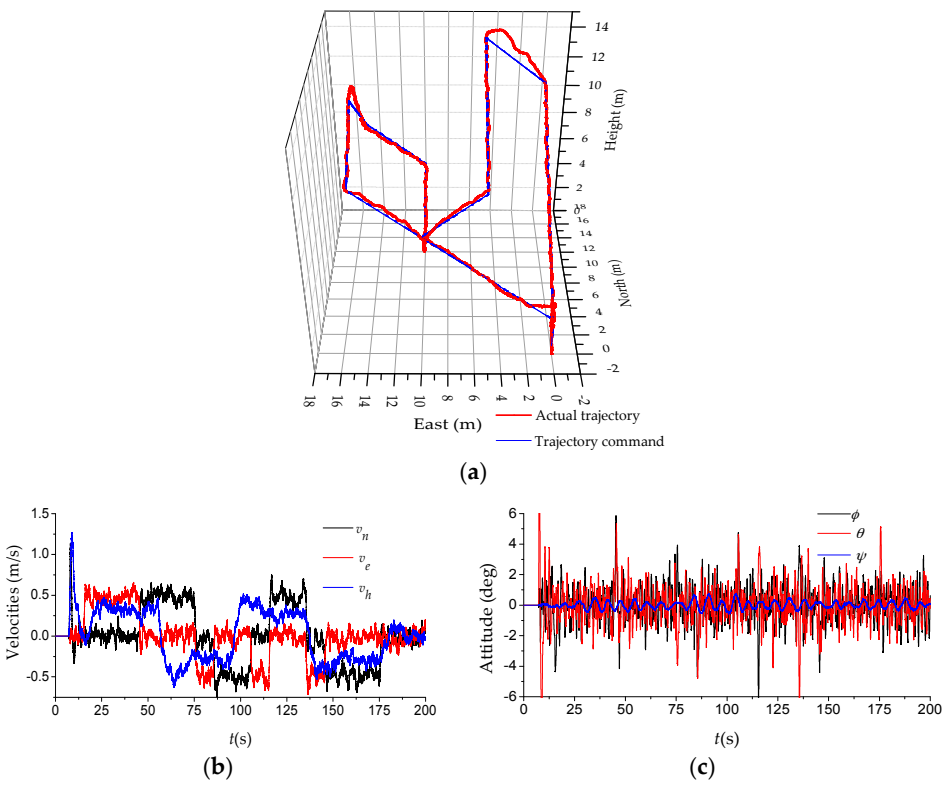

Figure 12. The experimental results of the conventional method during near-hover operations: (**a**) 3D flight trajectory tracking; (**b**) flight velocities; and (**c**) attitude.

Figure 12 shows the experimental results of the conventional method during near-hover operations. According to the experimental data, the deviation distance is more than 0.23 m during the straight line flight, and the height tracking error is more than 1.3 m, as shown in Figure 12a–c. The experimental results of the conventional method also demonstrate that the horizontal position error reaches a maximum value of 0.20 m, and height error also reaches a maximum value of 0.55 m in the presence of disturbances and uncertainties during the hovering flight.

Compared with the results of the proposed method, the resulting performance of the conventional method deteriorates significantly precisely because of the nonlinearity and the coupling interactions mentioned above, as demonstrated in [3,21]. From the comparison of the experimental results of two flight control methods, we can therefore conclude that the proposed method contributes to the significant improvement of the flight performance of the variable-pitch quadrotor, such as the endurance performance and the positioning accuracy.

7. Conclusions

To address the control and optimization problems of the electric variable-pitch quadrotor, a steady-state identification method to estimate the parameters of the mathematical model of the electric variable-pitch propeller has been first developed. A control and optimization strategy for the variable-pitch propeller, mainly including the steady-state control and optimization scheme with minimum power consumption, the adaptive compensation scheme and the cascade compensation scheme, is then proposed, which greatly improves the response performance of the lift force produced by the variable-pitch propeller. Furthermore, the direct lift-based flight control strategy is presented, which contributes to the improvement of the flight performance of the variable-pitch quadrotor, precisely because the roll, pitch, yaw and vertical channels are approximately linearized and completely decoupled from each other in this case. The experimental test results have comparatively demonstrated the efficiency and superiority of the proposed method. These achievements can also apply to other micro air vehicles with electric variable-pitch propellers.

Acknowledgments: This study was supported in part by National Natural Science Foundation of China (NSFC) (Under Grant No. 61374188), Natural Science Foundation of Jiangsu Province of China (Under Grant No. BK20141412), Applied Basic Research Programs of Natural Science Foundation of Jiangsu Province, China (Under Grant No. BY2015003-10). The authors would like to thank Professor Ben M. Chen in National University of Singapore for providing facilities and assistance.

Author Contributions: All authors discussed the contents of the manuscript. Shouzhao Sheng contributed to the research idea and the framework of this study. Chenwu Sun performed the experiments.

Conflicts of Interest: The authors declare no conflict of interest.

References

1. Altug, E.; Ostrowski, J.P.; Mahony, R. Control of a Quadrotor Helicopter Using Visual Feedback. In Proceedings of the 2002 IEEE International Conference on Robotics and Automation (ICRA), Washington, DC, USA, 10–17 May 2002; Volume 1, pp. 72–77.
2. Tayebi, A.; McGilvray, S. Attitude stabilization of a VTOL quadrotor aircraft. *IEEE Trans. Control Syst. Technol.* **2006**, *14*, 562–571. [CrossRef]
3. Madani, T.; Benallegue, A. Control of a Quadrotor Mini-Helicopter via Full State Backstepping Technique. In Proceedings of the 2006 45th IEEE Conference on Decision and Control, San Diego, CA, USA, 13–15 December 2006; pp. 1515–1520.
4. How, J.P.; Bethke, B.; Frank, A.; Dale, D.; Vian, J. Real-time indoor autonomous vehicle test environment. *IEEE Trans. Control Syst. Mag.* **2008**, *28*, 51–64. [CrossRef]
5. Pounds, P.; Mahony, R.; Corke, P. Modeling and control of a large quadrotor robot. *Control Eng. Pract.* **2010**, *18*, 691–699. [CrossRef]
6. Ryll, M.; Bulthoff, H.H.; Giordano, P.R. First Flight Tests for a Quadrotor UAV with Tilting Propellers. In Proceedings of the 2013 IEEE International Conference on Robotics and Automation (ICRA), Karlsruhe, Germany, 6–10 May 2013; pp. 295–302.

7. Sheng, S.; Sun, C. Design of a Stability Augmentation System for an Unmanned Helicopter Based on Adaptive Control Techniques. *Appl. Sci.* **2015**, *5*, 575–586. [CrossRef]
8. Sheng, S.; Sun, C. A Near-Hover Adaptive Attitude Control Strategy of a Ducted Fan Micro Aerial Vehicle with Actuator Dynamics. *Appl. Sci.* **2015**, *5*, 666–681. [CrossRef]
9. Sheng, S.; Sun, C.; Zhao, H. Indirect Adaptive Attitude Control for a Ducted Fan Vertical Takeoff and Landing Microaerial Vehicle. *Math. Probl. Eng.* **2015**, *2015*. [CrossRef]
10. Bouabdallah, S.; Murrieri, P.; Siegwart, R. Towards Autonomous Indoor Micro VTOL. *Auton. Robots* **2005**, *18*, 171–183. [CrossRef]
11. Bresciani, T. Modeling, Identification and Control of a Quadrotor Helicopter. Master's Thesis, Lund University, Lund, Sweden, 1 January 2008.
12. Shirsat, A.R. Modeling and Control of a Quadrotor UAV. Master's Thesis, Arizona State University, Tempe, AZ, USA, May 2015.
13. Erginer, B.; Altug, E. Modeling and PD control of a quadrotor VTOL vehicle. In Proceedings of the 2007 IEEE Intelligent Vehicles Symposium, Istanbul, Turkey, 13–15 June 2007; pp. 894–899.
14. Walid, M.; Slaheddine, N.; Mohamed, A.; Lamjed, B. Modeling and Control of a Quadrotor UAV. In Proceeding of the 2014 15th International Conference on Sciences and Techniques of Automatic Control and Computer Engineering (STA), Hammamet, Tunisia, 21–23 December 2014; pp. 343–348.
15. Alexis, K.; Nikolakopoulos, G.; Tzes, A. Model Predictive Quadrotor Control: Attitude, Altitude and Position Experimental Studies. *IET Control Theory Appl.* **2012**, *6*, 1812–1827. [CrossRef]
16. Kim, J.; Kang, M.S.; Park, S. Accurate Modeling and Robust Hovering Control for a Quad–Rotor VTOL Aircraft. In Proceeding of the Selected Papers from the 2nd International Symposium on UAVs, Reno, NV, USA, 8–10 June 2009; pp. 9–26.
17. Hoffmann, G.M.; Huang, H.; Waslander, S.L.; Tomlin, C.J. Quadrotor Helicopter Flight Dynamics and Control: Theory and Experiment. In Proceeding of the AIAA Guidance, Navigation, and Control Conference, Hilton Head, SC, USA, 21–22 August 2007; Volume 2.
18. Bouabdallah, S. Design and Control of Quadrotors with Application to Autonomous Flying. Ph.D. Thesis, Swiss Federal Institute of Technology, Lausanne, Switzerland, 10 January 2007.
19. Cutler, M.; Ure, N.K.; Michini, B.; How, J.P. Comparison of Fixed and Variable Pitch Actuators for Agile Quadrotors. In Proceeding of the AIAA Conference on Guidance, Navigation and Control and Co-Located Conferences (GNC), Portland, OR, USA, 8–11 August 2011. [CrossRef]
20. Cutler, M. Design and Control of an Autonomous Variable-Pitch Quadrotor Helicopter. Ph.D. Thesis, Massachusetts Institute of Technology, Cambridge, MA, USA, 23 August 2012.
21. Riccardi, F.; Panizza, P.; Lovera, M. Identification of the Attitude Dynamics for A Variable-Pitch Quadrotor UAV. In Proceeding of the European Rotorcraft Forum (ERF) 2014, Southampton, UK, 2–5 September 2014.
22. Fresk, E. Modeling, Control and Experimentation of a Variable Pitch Quadrotor. Master's Thesis, Luleå University of Technology, Luleå, Sweden, 2013.
23. Michini, B.; Redding, J.; Ure, N.K.; Cutler, M.; How, J.P. Design and Flight Testing of an Autonomous Variable-pitch Quadrotor. In Proceeding of the 2011 IEEE International Conference on Robotics and Automation (ICRA), Shanghai, China, 9–13 May 2011; pp. 2978–2979.
24. Cutler, M.; How, J.P. Actuator Constrained Trajectory Generation and Control for Variable-Pitch Quadrotors. In Proceeding of the AIAA Guidance, Navigation, and Control Conference (GNC), Minneapolis, MN, USA, 13–16 August 2012.
25. Bristeau, P.J.; Martin, P.; Salaun, E.; Petit, N. The Role of Propeller Aerodynamics in the Model of a Quadrotor UAV. In Proceeding of the European Control Conference, Budapest, Hungary, 23–26 August 2009.
26. Drela, M. QPROP Users Guide. 2009. Available online: http://web.mit.edu/drela/Public/web/qprop/ (accessed on 10 November 2015).
27. Hanselman, D.C. *Brushless Permanent Magnet Motor Design*, 2nd ed.; The Writers' Collective: Cranston, RI, USA, 2003.

© 2016 by the authors; licensee MDPI, Basel, Switzerland. This article is an open access article distributed under the terms and conditions of the Creative Commons by Attribution (CC-BY) license (http://creativecommons.org/licenses/by/4.0/).